processes

MDPI

Article

CO_2-Enhanced Gas Recovery in Offshore Carbon-Rich Gas Reservoirs—Part 1: In Situ Gas Dispersion Behaviors

Ping Jiang [1,2], Yuqiang Zha [1,2,*], Qing Ye [1,2], Runfu Xiong [1,2], Nan Zhao [1,2], Fengyang Mo [1,2], Lei Sun [3], Minxuan Li [1,2], Yuqi Zeng [3] and Bin Liang [3]

1 CNOOC China Limited, Hainan Branch, Haikou 570125, China; xiongrf@cnooc.com.cn (R.X.)
2 China National Offshore Oil Corporation (CNOOC) South China Sea Oil and Gas Energy Academician Workstation, Haikou 570125, China
3 State Key Laboratory of Oil and Gas Reservoir Geology and Exploitation, Southwest Petroleum University, Chengdu 610500, China; binliang@swpu.edu.cn (B.L.)
* Correspondence: zhayq@cnooc.com.cn

Abstract: In the middle and late stages of offshore carbon-rich gas reservoir development, insufficient reservoir energy poses significant challenges and difficulty in improving gas recovery. Injecting CO_2 back into the reservoir is a promising development approach that can address both carbon emissions and enhanced gas recovery (EGR). During the CO_2 injection process, the CO_2–CH_4 dispersion significantly impacts the recovery of CH_4. To understand the mass transfer and dispersion laws of CO_2 and high-carbon natural gas under current in situ reservoir conditions, this study conducted 1-m-long core experiments to investigate the effects of different gas compositions and permeabilities on gas recovery and diffusion laws in offshore reservoirs, taking into account the evolution of permeability in the porous medium. The experimental results indicate that the higher carbon concentration helps reduce mixing with formation gas, which consists of 70% methane, 25% nitrogen, and 5% carbon dioxide, resulting in a smaller diffusion coefficient. Under the conditions of an injection rate of 0.4 mL/min, a temperature of 81 °C, and a pressure of 7 MPa, the diffusion coefficient decreases by 27.5% as the carbon dioxide concentration increases from 70% to 90%, resulting in a 1.5% increase in recovery efficiency. As the permeability decreases, the viscous resistance of the fluid increases, leading to longer breakthrough times, and the reservoir fluid becomes more akin to piston displacement, reducing the degree of dispersion. The findings of this study provide guidance for optimizing gas injection strategies by reducing CO_2 dispersion and further enhancing natural gas recovery.

Keywords: CCUS; CO_2-EGR; offshore gas reservoir; dispersion

Citation: Jiang, P.; Zha, Y.; Ye, Q.; Xiong, R.; Zhao, N.; Mo, F.; Sun, L.; Li, M.; Zeng, Y.; Liang, B. CO_2-Enhanced Gas Recovery in Offshore Carbon-Rich Gas Reservoirs—Part 1: In Situ Gas Dispersion Behaviors. *Processes* **2024**, *12*, 2479. https://doi.org/10.3390/pr12112479

Academic Editor: Raymond Cecil Everson

Received: 7 October 2024
Revised: 30 October 2024
Accepted: 31 October 2024
Published: 8 November 2024

1. Introduction

The urgent sustainable development of human society requires improving the energy structure, particularly through developing and utilizing clean and new energy sources. Natural gas, as a clean and low-carbon fossil fuel, plays an increasingly significant role in the global energy consumption structure [1–3]. With its high calorific value and low carbon emissions, natural gas can help reduce carbon emissions. Therefore, the efficient development and utilization of gas reserves are of great significance for ensuring energy security, promoting green economic development, and achieving carbon neutrality [4]. Depletion development is the primary method for gas reservoir exploitation. In the later stages of gas field development, insufficient energy within the reservoir leads to a significant portion of natural gas remaining trapped. Additionally, gas reservoirs with underlying water face challenges of water influx in the later stages of development. Effectively controlling water influx is a pressing issue that needs to be addressed in developing water-bearing gas reservoirs [5]. Injecting CO_2 into depleted and partially depleted gas reservoirs can enhance gas recovery and facilitate CO_2 storage in the reservoir due to the differences in

properties between CO_2 and natural gas. Additionally, injecting CO_2 at the gas-water interface leads to CO_2 dissolution in water, increases reservoir pressure, and forms a foam zone to suppress water influx under certain conditions. Injecting CO_2 into the reservoir holds promising prospects for improving the hydrocarbon recovery in depleted gas reservoirs [6]. In addition to CO_2, nitrogen, water, and some light hydrocarbons are also injected into gas reservoirs to enhance recovery. It is worth noting that water and light hydrocarbon injections are generally only applied in gas condensate reservoirs [7–10].

After the concept of CO_2 storage with enhanced gas recovery (CSEGR or CO_2-EGR) was proposed [11], researchers conducted studies on the economic and technical feasibility of injecting CO_2 into reservoirs [12]. Technically, injecting CO_2 into reservoirs is feasible, but it can contaminate natural gas. For the majority of gas reservoirs, CO_2 storage is considered after the reservoir is abandoned. During the process of injecting CO_2, the injected gas mixes with natural gas. The diffusion behavior and displacement effect of the gas affects the gas recovery rate. Therefore, the diffusion and dispersion behaviors of CO_2 in natural gas reservoirs are a key focus of CO_2-EGR research [13,14].

When CO_2 is injected into gas reservoirs, changes in temperature and pressure occur with increasing depth in the geological formations. These variations cause a widening gap in the physical properties between CO_2 and CH_4 [6], thereby affecting their flow characteristics within the reservoir. Experts in petroleum studies, such as Liu et al. (2015, 2020), studied the dispersion coefficient at different pressures (4–30 MPa) and temperatures (60–150 °C) [15,16]; Sidiq and Amin et al. (2009) studied the dispersion coefficient at different pressures (10–40 MPa) and 160 °C [17]; and Seo and Mamora et al. delved deep into the effects of pressure and temperature on the dispersion coefficients of CO_2–CH_4 [13]. Their findings indicate that rising temperature enhances intermolecular diffusion, leading to larger diffusion coefficients for CO_2 and CH_4. Prior to CO_2 reaching its critical pressure of 7.38 MPa, the dispersion coefficient increases with injection pressure. When the pressure exceeds the critical pressure, causing CO_2 to become supercritical, the dispersion coefficient decreases with increasing pressure. Additionally, subsequent studies by Sidi and Amin et al. (2012) [18] explored the recovery rate of CO_2–CH_4 mixed gas under different injection pressures. The results of these studies demonstrate that increasing pressure significantly amplifies the differences in physical properties between CO_2 and CH_4, thereby influencing their degree of mixing and further enhancing gas recovery. Apart from the effect of pressure and temperature, Abba et al. found that increasing the injection rate of CO_2 at 8.96 MPa and 40 °C to 50 °C would cause CO_2 to break through earlier. At an injection rate of 0.2 to 0.4 mL/min, the horizontal displacement CO_2 dispersion coefficient, due to gravity segregation, is greater than the vertical dispersion coefficient. However, when the rate reaches 0.5 mL/min, this difference becomes less noticeable [19]. Liu investigated the impact of the injection rate on the dispersion coefficient and showed that as the injection rate increases, the convection of CO_2–CH_4 is more intense, thereby increasing the dispersion coefficient [6,19]. Scholars also studied the relationship between permeability and the dispersion coefficient. In their experiments, the general trend is that the greater the permeability, the smaller the dispersion coefficient. An explanation for the phenomenon is that the flow channels tend to be more tortuous when the permeability decreases, which in turn leads to a higher degree of CO_2–CH_4 miscibility [20,21]. However, Honari et al. observed an abnormal phenomenon where a larger dispersion coefficient occurred in cores with greater permeability [22]. Therefore, the relationship between permeability and the dispersion coefficient still requires further exploration.

Regarding injection gas components, Nogueira et al. studied the extent to which impurity components in flue gas (nitrogen, oxygen, water, sulfur dioxide, carbon monoxide, etc.) affect the displacement of natural gas by CO_2 [23]. Turta et al. and Sim et al. studied the effects of different lengths of cores and injected gas components on the recovery of CH_4 at low pressure but unfortunately failed to fully simulate the actual gas reservoir [24,25]. Some researchers altered the concentration of CH_4 in the formation gas to investigate the effectiveness of CO_2 displacement under different formation gas conditions [17,26].

Mohammed et al. (2020) used N_2 as a buffer gas, injecting N_2 before CO_2 to study the barrier mechanism of N_2 in CO_2–CH_4, and the results showed that N_2 can effectively prevent the miscibility of CO_2 with CH_4, which is beneficial for the sequestration of CO_2 [27]. Zhang Y et al. (2022) utilized a CO_2 + N_2 system as the injection gas to displace natural gas [21], studying the seepage characteristics of CO_2–CH_4. The results indicated that N_2 is more likely to mix with CH_4, and there is an optimal injection rate for N_2 beyond which the recovery rate decreases. However, the concentration of CO_2 in the injected gas was not compared. To find a preferable CO_2 concentration to enhance the recovery rate of natural gas, it is necessary to study the seepage characteristics of injecting different concentrations of CO_2 in natural gas reservoirs.

The efficiency of CO_2 displacement is a crucial factor in assessing the effectiveness of gas flooding. Wei et al. investigated the impact of different concentrations of CO_2 on enhancing the recovery rate in coalbeds. Their findings indicate that pure CO_2 yields a higher recovery rate and a later breakthrough time compared to a mixture of N_2 and CO_2 [28]. Pooladi-Darvish et al. and their team injected a low-pressure gas system of CO_2 and H_2S into the reservoir. They observed that CO_2 and H_2S broke through within 1 to 3 years after injection, suggesting that under low-pressure conditions, the injection of gases that are not significantly different from the formation gas can accelerate the mixing process, leading to an earlier breakthrough of the gases [29].

As shown in Figure 1, the Central Diapir Zone serves as the primary area for gas production and reserves in the Yinggehai Basin, with the Dongfang area situated within this zone [30]. Recently, Dongfang offshore gas reservoirs of CNOOC, which are typical carbon-rich gas reservoir, have been implementing CO_2-EGR practice on a reservoir scale. The average permeability of the Dongfang gas reservoir is approximately 20 mD, with a high carbon content in the produced gas. In some gas wells, the carbon content reaches up to 80%. A key measure in Dongfang practice is injecting produced gas directly or partially purified back into the reservoir. Negligible content of CH_4 exists in the injection gas. The dispersion behavior of such gas in natural gas reservoirs is not understood. In consideration of this, we examined the dispersion behavior of CO_2 with CH_4 in natural gas reservoirs under varying injection gas concentrations, permeabilities, and injection rates, alongside methane recovery. By comparing dispersion coefficients across different conditions, we revealed the influencing factors of CO_2 displacing CH_4 and its dispersion characteristics within porous media. These findings are expected to guide CO_2-EGR in carbon-rich offshore gas reservoirs.

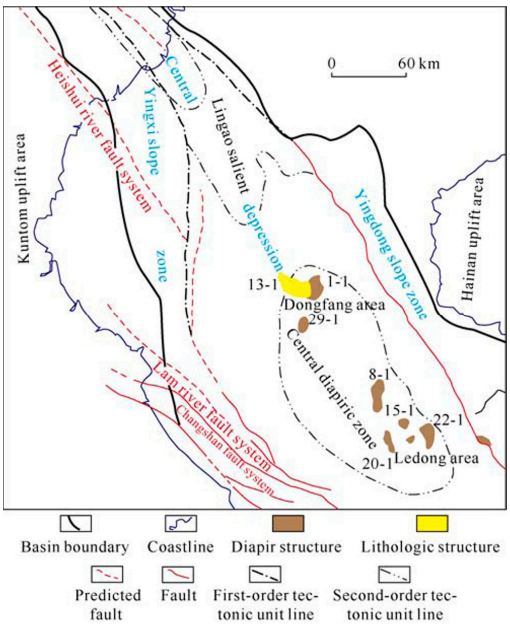

Figure 1. Tectonic units of the Yinggehai Basin [30].

2. Dispersion Theory

The dispersion process can be considered to be composed of molecular diffusion and mechanical dispersion. Molecular diffusion results from the flow phenomenon caused by concentration gradients, and gas diffusion is generally stronger than that of liquids. Mechanical dispersion occurs when fluid flows through porous media at non-uniform velocities within the pores. This velocity gradient in the flow direction causes dispersion of the fluid, known as longitudinal dispersion. Additionally, due to the influence of the tortuosity of the porous media, fluid dispersion occurs perpendicular to the flow direction, known as transverse dispersion [31]. Molecular diffusion is independent of flow velocity. Together, they determine the overall effect of substance transport in porous media, known as total dispersion. The combined effects of both can be described by the total dispersion coefficient.

Overall, the dispersion process is the result of the combined effects of molecular diffusion and mechanical dispersion. Generally, when the Peclet number (Npe) is small (<0.1), molecular diffusion dominates the dispersion process. When Npe is large (Npe > 10), mechanical dispersion becomes predominant, and molecular diffusion can be negligible. When the dispersion coefficient falls within this range, both molecular diffusion and mechanical dispersion play a significant role in the dispersion process. In the transition region between the two, both molecular diffusion and mechanical dispersion play significant roles and cannot be ignored [31,32].

Transverse dispersion coefficients are often neglected due to being significantly smaller than longitudinal dispersion coefficients. Therefore, one-dimensional convection-dispersion equations are commonly used to characterize dispersion problems. As shown in Figure 2, the breakthrough curve of CO_2 resembles a normal distribution and requires two conditions to be met: (1) homogeneous rock cores, and (2) injection gas density and viscosity should be similar to reservoir gas density and viscosity [33].

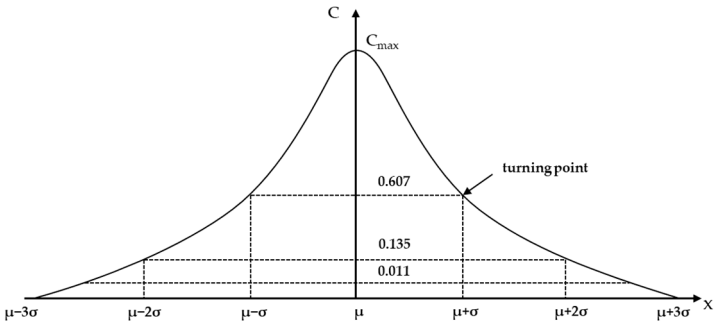

Figure 2. Normal distribution of concentration.

The method generally used for laboratory measurement of dispersion coefficients is the breakthrough column method, similar to oil displacement experiments with core samples. When the displacement front reaches the outlet, the injected fluid concentration rapidly increases from 0 to 1 due to dispersion effects. The partial concentration at the outlet can be fitted to calculate Npe and dispersion coefficients.

The initial boundary value problem for one-dimensional transport consists of the following equation and appropriate initial and boundary conditions. For transport in a semi-infinite medium, the initial boundary value problem consists of the following set of equations:

$$\frac{\partial C}{\partial t} + \mu_x \frac{\partial C}{\partial x} - D_L \frac{\partial^2 C}{\partial x^2} = 0 \quad (1)$$

$$C(x, 0) = C_i \quad (2)$$

$$C(0, t) = C_j \quad (3)$$

$$C(\infty, t) = C_i \quad (4)$$

Ogata and Banks (1961) provided a solution to the above equations.

$$C(x,t) = \frac{C_j}{2}\left[\operatorname{erfc}\left(\frac{x-u_x t}{2\sqrt{D_L t}}\right) + e^{\frac{u_x x}{D_L}}\operatorname{erfc}\left(\frac{x+u_x t}{2\sqrt{D_L t}}\right)\right] \tag{5}$$

$$Npe = \frac{qL}{A\phi D_L} \tag{6}$$

Here, C represents mass concentration; C_i denotes the concentration of injected gas in the reservoir fluid at time $t = 0$; C_j signifies the concentration of the solvent at the inlet boundary condition; μ_x denotes the solvent pore velocity in the x direction; x stands for distance; t represents time, in minutes; D_L is the longitudinal dispersion coefficient, in cm^2/s; Npe stands for the Peclet number; A denotes the cross-sectional area of the core, in cm^2; q is the injection flow rate, in ml/min; L represents the length of the core, in cm; and Φ represents porosity.

D_L is calculated using the following equation:

$$D_L = \frac{1}{8}\left[\frac{x-u_x t_{0.1587}}{\sqrt{t_{0.1587}}} - \frac{x-u_x t_{0.8413}}{\sqrt{t_{0.8413}}}\right]^2 \tag{7}$$

In general, the width of the transition zone is much smaller compared to the length of the core, thus we have the following:

$$\begin{aligned} t_{0.5} - t_{0.1587} &<< t_{0.5} \\ t_{0.8413} - t_{0.5} &<< t_{0.5} \end{aligned} \tag{8}$$

The values of $t_{0.1587}$ and $t_{0.8413}$ in the above equation can be replaced with $t_{0.5}$, yielding the following:

$$D_L = \frac{{u_x}^2}{8t_{0.5}}(t_{0.8413} - t_{0.1587})^2 \tag{9}$$

$$\mu_x = \frac{q}{A\phi} \tag{10}$$

3. Experimental Materials and Procedure

3.1. Cores and Fluids

The experimental cores and fluid samples were obtained from the Dongfang gas field. The basic parameters of the cores are listed in Table 1. As the cores are loose, the whole body of each core is wrapped with lead, and the two ends are fixed with steel wire filters to prevent sanding, as shown in Figure 3. However, due to the loose nature of the core, we observed a gradual evolution of the core permeability during the experimental process. After each experiment, the permeability gradually decreased, and after six experiments, it dropped from the initial 14.62 mD to 0.97 mD. Table 2 lists the experimental scheme and the evolution of the permeability during each experiment.

Table 1. Basic parameters of experimental cores.

No.	Length cm	Diameter cm	Permeability mD	Porosity %
DF1-1-5	4.93	2.54	17.64	32.19
DF1-1-7	4.98	2.54	17.28	30.36
DF1-1-48	5.09	2.54	14.68	34.00
DF1-1-8	4.88	2.54	16.65	33.65
DF1-1-9	4.78	2.54	15.89	34.25
DF1-1-10	4.89	2.55	15.80	35.01
DF1-1-11	4.88	2.54	16.52	32.25
DF1-1-12	4.77	2.53	16.51	34.77

Table 1. *Cont.*

No.	Length cm	Diameter cm	Permeability mD	Porosity %
DF1-1-52	5.01	2.54	15.23	33.89
DF1-1-60	4.95	2.54	14.90	34.39
DF1-1-15	4.88	2.53	16.39	31.88
DF1-1-16	4.88	2.54	16.12	36.24

Figure 3. Image of the rock samples.

Table 2. Experimental scheme and the permeability evolution of the composite long core.

No.	Development Scheme	Objective	Evolutive Permeability mD
1#	14 MPa → 7 MPa	-	14.62
2#	14 MPa → 5 MPa, 5 MPa → 7 MPa	1#/2# compare the effect of depleted development pressure	6.65
3#	14 MPa → 5 MPa, 5 MPa → 7 MPa	2#/3# compare the effect of permeability	3.9
4#	14 MPa → 7 MPa	1#/4#/5#/6# compare the effect of the injected gas composition	3.0
5#	14 MPa → 7 MPa		1.7
6#	14 MPa → 7 MPa		0.97

The experimental fluid was reconstituted in the laboratory according to the formation pressure of 14 MPa and the formation temperature of 81 °C, with the composition of the formation fluid detailed in Table 3. The injected fluid was reconstituted according to the formation pressure of 7 MPa and the formation temperature of 81 °C, with the composition of the injected fluid detailed in Table 4.

Table 3. Composition of formation gas.

Component	Composition, mol%
CH_4	70
N_2	25
CO_2	5

Table 4. Composition of injected gas.

Component	Composition, mol%		
CH_4	10	30	50
N_2	0	0	0
CO_2	90	70	50

3.2. Experimental Procedure

The experimental process began with a depletion experiment conducted on a long core sample, followed by a constant-pressure displacement experiment. These experiments were designed to investigate the gas flow behavior during gas injection and the diffusion mechanism of CO_2 in CH_4. The experimental temperature was maintained at the reservoir temperature of 81 °C. The main experimental equipment is as follows: a displacement pump (P11-03-03) with a pressure accuracy of 0.5%. A multifunctional long core displacement apparatus (NSPTHX-1203) provides a pressure accuracy of ±1 psi and a temperature accuracy of ±0.1 °C. A gas metering device (NSPTQLY) with a volumetric error of 5% was used to collect the produced gas at the outlet. A gas chromatograph (7890B, Agilent Technologies, Santa Clara, CA, USA) was used to analyze the composition of the collected gas samples. The experimental flowchart is shown in Figure 4.

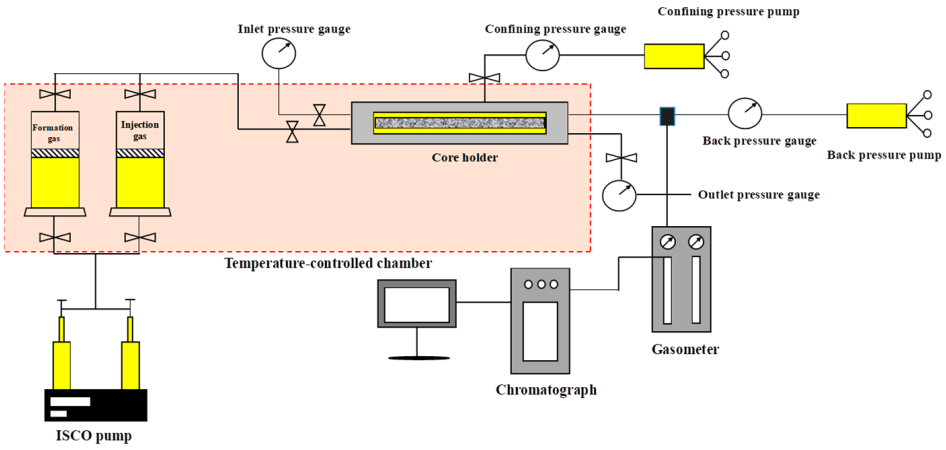

Figure 4. Schematic diagram of experimental equipment.

The experimental procedure is as follows: The core samples were first dried and their permeability was measured. After calculating the core arrangement based on the results, the long-core holder was loaded with the ordered cores. The assembled long core was then vacuumed for 24 h. The core sample parameters are listed in Table 1. Then, an initial confining pressure of 3 MPa was applied, and the pre-prepared formation fluid was injected into the long core using a high-precision displacement pump. Concurrently, the confining pressure, injection pressure, and back pressure were gradually increased, ensuring that the confining pressure was always at least 2 MPa higher than the injection pressure. The internal pressure of the core was gradually raised to a formation pressure of 14 MPa. At a formation pressure of 14 MPa, the permeability of the assembled long core was measured. Depletion-style depressurization was carried out using two pressure schemes. In the first scheme, 14 MPa → 7 MPa, the back pressure at the outlet was gradually reduced to 7·MPa. The produced gas was collected and measured using a gas-metering device at the outlet. Once the pressure reached 7 MPa, the fluid specified in Table 3 was injected into the long core at a controlled rate, ensuring constant-pressure displacement at 7 MPa. In the second scheme, 14 MPa → 5 MPa → 7 MPa, the pressure in the long core was first depleted to 5 MPa, then raised to 7 MPa without gas production. Subsequent gas injection was conducted at 7 MPa. For every 0.05 pore volume (PV) of fluid injected, the produced fluid at the outlet was analyzed using gas chromatography. The experiment concluded when the

composition of the produced fluid became consistent with that of the injected fluid, with no further changes in chromatographic results.

4. Results and Discussion

4.1. EGR and CO_2 Breakthrough

During the experiments, CO_2 displacement experiments for CH_4 were conducted under conditions of 81 °C and 7 MPa, with a displacement rate of 4×10^{-3}~5×10^{-3} cm/s. The recovery of CH_4 was compared across different injected gas compositions (90% CO_2 + 10% CH_4, 70% CO_2 + 30% CH_4, 50% CO_2 + 50% CH_4) in cores with varying permeability. Before the CO_2 injection, depletion experiments were first conducted to simulate the primary recovery process. The depletion process resembled a constant-volume depletion. The degree of depletion recovery is shown in Figure 5. Subsequent gas injection displacement experiments explored the displacement process in cores with different permeability levels of 14.62 mD, 6.65 mD, 3.9 mD, 3 mD, 1.7 mD, and 0.97 mD. The CO_2 breakthrough curves at the outlet, under varying injected gas concentrations and permeability, are displayed in Figure 6, while the recovery rate comparisons are displayed in Figure 7. The effects of different injected gas compositions, permeability, displacement rates, and Peclet numbers on the diffusion behaviors are also addressed.

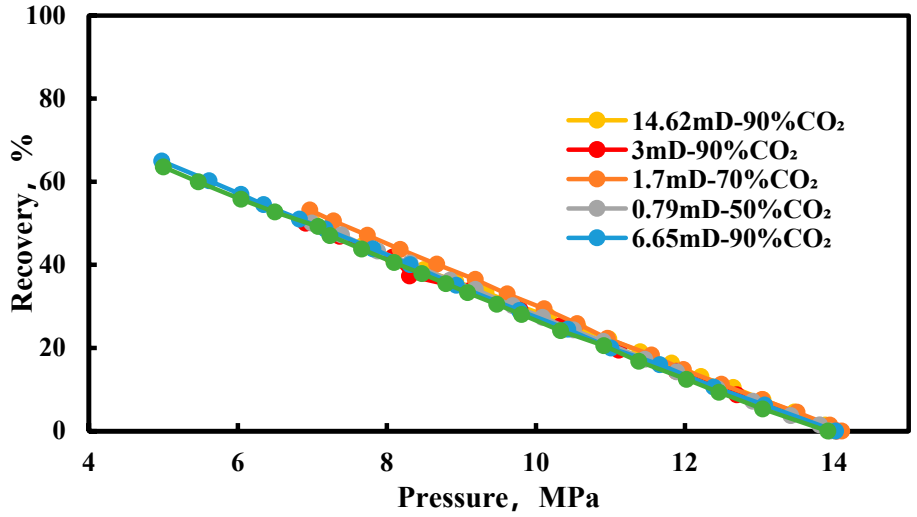

Figure 5. Recovery curves of depletion developments.

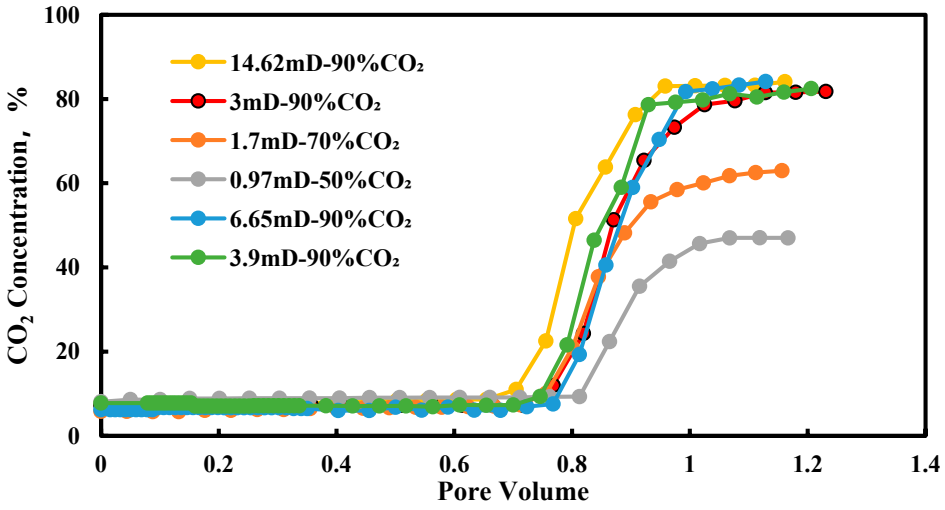

Figure 6. CO_2 breakthrough curves at different injected gas concentrations and permeabilities.

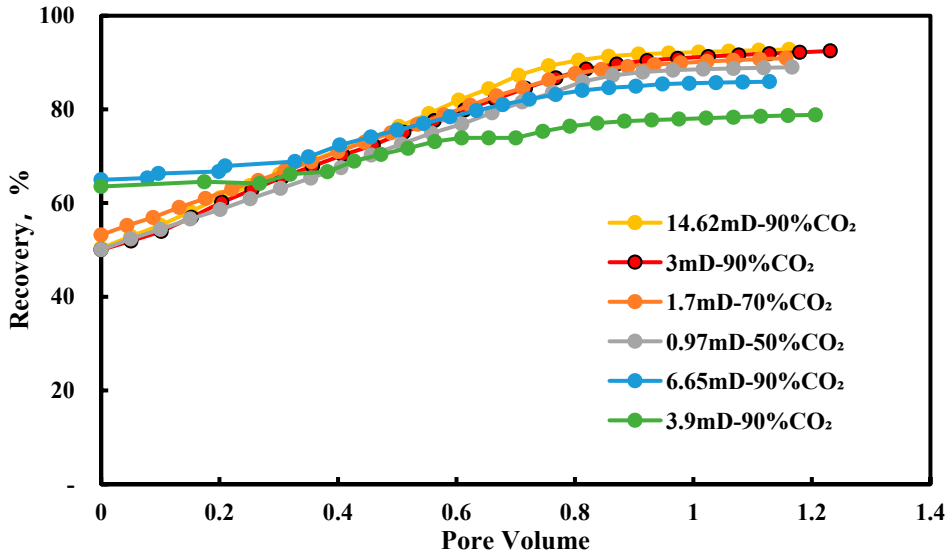

Figure 7. Recovery at different injected gas concentrations and permeabilities.

Figure 6 illustrates that, during the early stage of the displacement experiment, the CO_2 concentration of the produced gas matches the CO_2 content in the formation gas. As the displacement progresses, the injected gas reaches the outlet and CO_2 concentration rapidly increases. At around 1 pore volume (PV), the rise in CO_2 concentration begins to level off. The higher the concentration of CO_2 in the injected gas, the earlier the breakthrough point occurs. Due to the combined effects of permeability and injected gas concentration, there are slight variations in the breakthrough point. However, higher permeability tends to facilitate the earlier breakthrough of injected CO_2. Based on the analysis of the curves in Figures 6 and 7, it can be concluded that a higher CO_2 concentration in the injected gas leads to better miscibility between the injected gas and formation gas, resulting in a shorter transition zone in the breakthrough curve and a higher gas recovery accordingly. Figure 8 provides the recovery of different experiments. A comparison of the 14.62 mD and 6.9 mD cases indicates that the pressure increase in the 14 MPa → 5 MPa → 7 MPa scheme decreases the final recovery. The difference in the recovery between the 6.65 mD case and the 3.9 mD case shows that permeability has a significant effect on recovery under the 14 MPa → 5 MPa → 7 Mpa scheme. A possible explanation for this is that the pressure-building process accelerates the mixing of CO_2 and formation gas, and the recovery of the remaining gas is more sensitive to permeability changes compared to 14 MPa → 7 MPa.

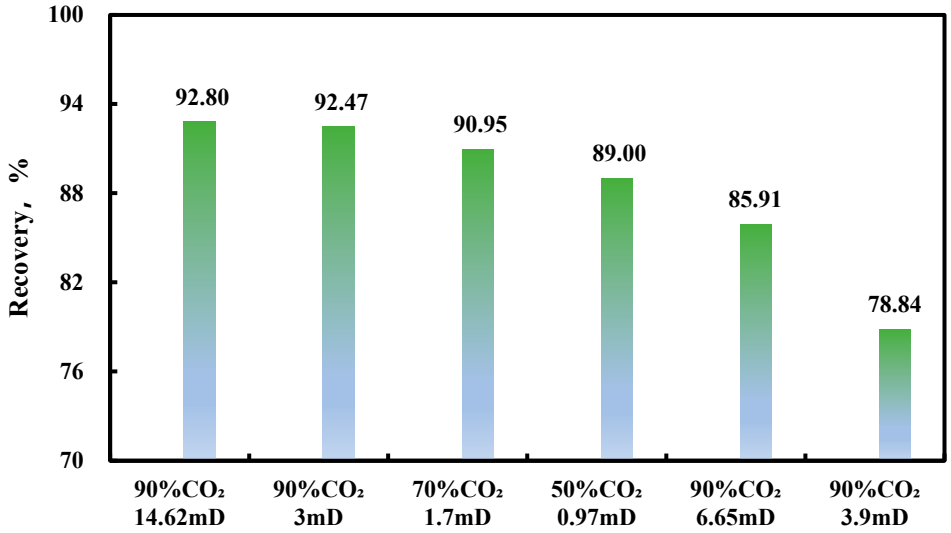

Figure 8. Gas recovery of different experiments.

4.2. CO_2 Dispersion Behaviors

During the gas displacement process, the diffusion between molecules will accelerate the movement of CO_2, enhance the mixing of CO_2 with natural gas, and thus affect the recovery rate. When CO_2 is injected into the reservoir, it first contacts the natural gas in the formation. Due to the concentration difference between the two, molecular diffusion predominantly occurs initially until the system reaches equilibrium. Molecular diffusion causes the appearance of a mixed-phase region, which harms the displacement efficiency of natural gas. As shown in Figure 6, the breakthrough point is 0.6~0.8 PV, caused by molecular diffusion. During the experiment, with an injection rate of 4×10^{-3} cm/s, the dispersion coefficients calculated for the injection gas compositions of 90% CO_2 + 10% CH_4 and 70% CO_2 + 30% CH_4 under a temperature of 81 °C and a pressure of 7 MPa were 0.680×10^{-3} cm^2/s and 0.938×10^{-3} cm^2/s, respectively. It can be observed that the lower the CO_2 concentration in the injection gas system, the higher the dispersion coefficient. This is because, with a lower CO_2 concentration and a higher CH_4 concentration, the injection gas composition is closer to that of the formation gas, which is more likely to lead to miscibility, resulting in a longer transition zone and more severe dispersion.

Permeability also affects the diffusion process. With a 90% CO_2 injection gas concentration and a displacement rate of 5×10^{-3} cm/s, after depleting to 5 MPa and then increasing the pressure to 7 MPa for constant pressure displacement, the dispersion coefficients for cores with permeabilities of 6.65 mD and 3.9 mD were 0.123×10^{-3} cm^2/s and 0.107×10^{-3} cm^2/s, respectively. As the permeability decreases, the dispersion coefficient also decreases. This is because, as the permeability decreases, the viscous resistance of the fluid increases, and the formation fluid is more likely to be displaced in a piston-like manner, reducing the degree of dispersion.

Table 5 lists the dispersion coefficients calculated for different experiments. By altering the injection rate, it was observed that as the injection rate increases, so does the dispersion coefficient, and the dispersion coefficient is quite sensitive to changes in the injection rate. The Peclet number (Npe) in porous media is an important factor reflecting the dispersion process. When Npe is typically lower than 0.1, the dispersion coefficient is predominantly determined by molecular diffusion, where molecular diffusion is much greater than the mechanical dispersion caused by convection. When Npe is higher than 10, the dispersion is dominated by mechanical dispersion, and molecular diffusion can be neglected. It can be seen in Figure 9 that there is a positive correlation between the injection rate and the dispersion coefficient. This is because an increase in the injection rate promotes convection between CO_2 and the formation gas, resulting in a larger dispersion coefficient. Figure 10 shows that when the injection rate is constant, there is a negative correlation between Npe and the dispersion coefficient. That is, the larger the Npe, the smaller the dispersion coefficient, which results in a steeper CO_2 breakthrough curve. Conversely, the smaller the Npe, the larger the dispersion coefficient, leading to a longer transition zone in the CO_2 breakthrough curve and a more gradual slope.

Table 5. Dispersion coefficients for different experiments.

Number	CO_2 Content of Injected Gas	Darcy Velocity 10^{-3} cm/s	Permeability mD	Npe	Dispersion Coefficient 10^{-3} cm^2/s
1#	90%	4.991	14.62	290	1.012
4#	90%	3.993	3	360	0.680
5#	70%	3.993	1.7	261	0.938
6#	50%	4.991	0.97	268	1.141
2#	90%	4.991	6.65	238	1.232
3#	90%	4.991	3.9	274	1.070

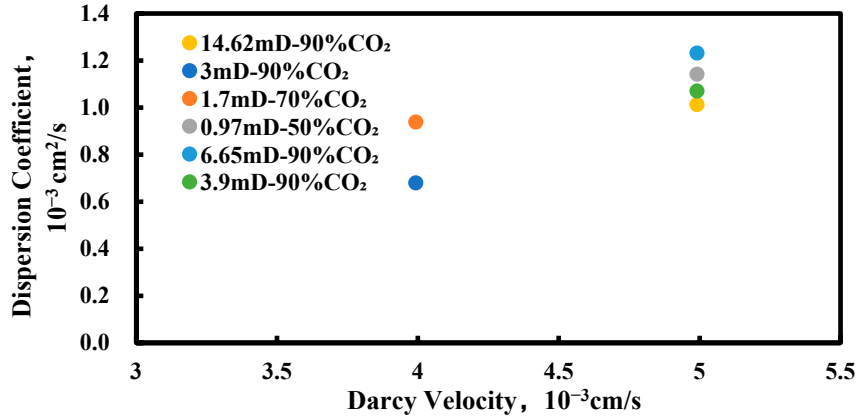

Figure 9. Dispersion coefficient versus velocity.

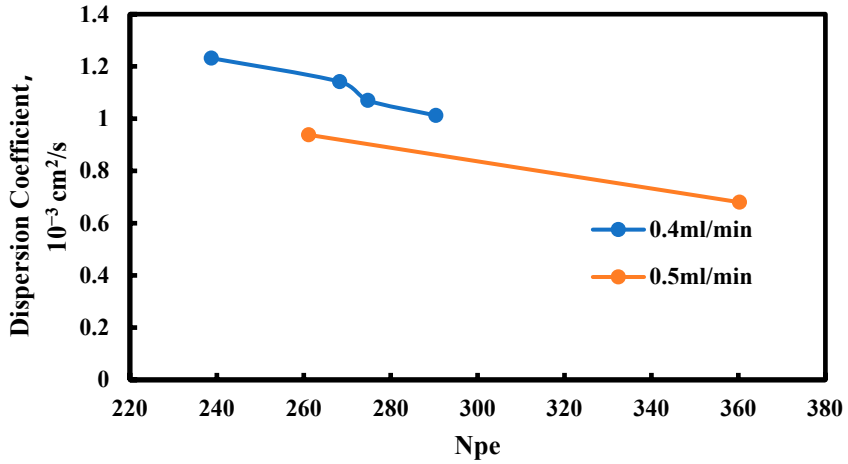

Figure 10. Relationship between Npe and dispersion coefficient.

5. Conclusions

This study investigated the effects of different gas compositions and permeability on gas diffusion behavior in offshore reservoirs by injecting produced CO_2 back into the reservoir. The impact of injection gas composition and permeability on the dispersion coefficient was analyzed and compared. The main conclusions are as follows.

1. The higher the concentration of CO_2 in the injected gas, the later the breakthrough time of CO_2, the shorter the transition zone, and the smaller the dispersion coefficient. The average dispersion coefficient is about 1×10 cm^3/s under the experimental conditions of this study. Additionally, both the breakthrough time of CO_2 and the recovery of CH_4 are influenced by permeability.
2. The higher the concentration of CO_2 in the injected gas, the greater the difference in physical properties between the injected gas and the formation gas, making it less likely to achieve miscibility and thus resulting in a smaller dispersion coefficient.
3. As the permeability decreases, the viscous resistance of the fluid increases, leading to a short transition zone. The formation fluid is more likely to be displaced in a piston-like manner, reducing the degree of dispersion. Besides analyzing the CO_2 breakthrough curve, more advanced techniques should be used to characterize the transition zone in greater depth and quantitatively.
4. Npe is inversely proportional to the dispersion coefficient. The longer the transition zone of the CO_2 breakthrough curve, the larger the Npe and the smaller the dispersion coefficient. Conversely, the shorter and steeper the transition zone of the CO_2 breakthrough curve, the smaller the Npe and the larger the dispersion coefficient.

Author Contributions: Conceptualization, Y.Z. (Yuqiang Zha); methodology, R.X. and B.L.; validation, Q.Y.; formal analysis, M.L. and N.Z.; investigation, Y.Z. (Yuqi Zeng) and B.L.; resources, P.J. and L.S.; data curation, F.M.; writing—original draft preparation, B.L. and Y.Z. (Yuqi Zeng); writing—review and editing, Y.Z. (Yuqiang Zha) and L.S.; visualization, F.M.; supervision, Q.Y. and L.S.; project administration, Y.Z. (Yuqiang Zha) and B.L.; funding acquisition, P.J. and R.X. All authors have read and agreed to the published version of the manuscript.

Funding: This research is supported by CNOOC South China Sea Oil & Gas Energy Academician Workstation (KJZH-2023-2203).

Data Availability Statement: Data will be available on request.

Conflicts of Interest: Authors Ping Jiang, Yuqiang Zha, Qing Ye, Runfu Xiong, Nan Zhao, Fengyang Mo and Minxuan Li were employed by the company China National Offshore Oil Corporation (CNOOC). The remaining authors declare that the research was conducted in the absence of any commercial or financial relationships that could be construed as a potential conflict of interest.

References

1. Ahmed, M.; Shuai, C.; Ahmed, M. Analysis of energy consumption and greenhouse gas emissions trend in China, India, the USA, and Russia. *Int. J. Environ. Sci. Technol.* **2023**, *20*, 2683–2698. [CrossRef]
2. Li, Q.; Li, Q.; Wang, F.; Wu, J.; Wang, Y. The carrying behavior of water-based fracturing fluid in shale reservoir fractures and molecular dynamics of sand-carrying mechanism. *Processes* **2024**, *12*, 2051. [CrossRef]
3. Li, Q.; Li, Q.; Han, Y. A numerical investigation on kick control with the displacement kill method during a well test in a deep-water gas reservoir: A case study. *Processes* **2024**, *12*, 2090. [CrossRef]
4. Zou, C.; Yang, Z.; He, D.; Wei, Y.; Li, J.; Jia, A.; Chen, J.; Zhao, Q.; Li, Y.; Li, J.; et al. Theory, technology and prospects of conventional and unconventional natural gas. *Pet. Explor. Dev.* **2018**, *45*, 604–618. [CrossRef]
5. Hamza, A.; Hussein, I.A.; Al-Marri, M.J.; Mahmoud, M.; Shawabkeh, R.; Aparicio, S. CO_2 enhanced gas recovery and sequestration in depleted gas reservoirs: A review. *J. Petrol. Sci. Eng.* **2021**, *196*, 107685. [CrossRef]
6. Liu, S.; Yuan, L.; Zhao, C.; Zhang, Y.; Song, Y. A review of research on the dispersion process and CO_2 enhanced natural gas recovery in depleted gas reservoir. *J. Petrol. Sci. Eng.* **2022**, *208*, 109682. [CrossRef]
7. Hussain, M.; Sidiq, A. Nitrogen injection for enhanced gas recovery in natural gas reservoirs. In Proceedings of the SPE Asia Pacific Oil and Gas Conference and Exhibition, Brisbane, QLD, Australia, 18–20 October 2010. [CrossRef]
8. Babadagli, T.; Al-Bemani, A.S. Waterflooding in gas condensate reservoirs: A review of recovery mechanisms and laboratory data. *J. Petrol. Sci. Eng.* **2001**, *29*, 133–144.
9. Orr, F.M., Jr.; Jessen, K. Uncertainties in gas injection for enhanced hydrocarbon recovery. *SPE J.* **2007**, *12*, 531–535.
10. Tananykhin, D.S.; Struchkov, I.A.; Khormali, A.; Roschin, P. Investigation of the influences of asphaltene deposition on oilfield development using reservoir simulation. *Pet. Explor. Dev.* **2022**, *49*, 1138–1149. [CrossRef]
11. van der Burgt, M.J.; Cantle, J.; Boutkan, V.K. Carbon dioxide disposal from coal-based IGCC's in depleted gas fields. *Energy Convers. Manag.* **1992**, *33*, 603–610. [CrossRef]
12. Oldenburg, C.M.; Stevens, S.H.; Benson, S.M. Economic feasibility of carbon sequestration with enhanced gas recovery (CSEGR). *Energy* **2004**, *29*, 1413–1422. [CrossRef]
13. Seo, J.G.; Mamora, D.D. Experimental and simulation studies of sequestration of supercritical carbon dioxide in depleted gas reservoirs. *J. Energy Resour. Technol.* **2005**, *127*, 1–6. [CrossRef]
14. Van Der Meer, B. Carbon dioxide storage in natural gas reservoir. *Oil Gas Sci. Technol. Rev. IFP* **2005**, *60*, 527–536. [CrossRef]
15. Liu, S.; Zhang, Y.; Xing, W.; Jian, W.; Liu, Z.; Li, T.; Song, Y. Laboratory experiment of CO_2–CH_4 displacement and dispersion in sandpacks in enhanced gas recovery. *J. Nat. Gas Sci. Eng.* **2015**, *26*, 1585–1594. [CrossRef]
16. Liu, S.; Zhang, Y.; Zhao, J.; Jiang, L.; Song, Y. Dispersion characteristics of CO_2 enhanced gas recovery over a wide range of temperature and pressure. *J. Nat. Gas Sci. Eng.* **2020**, *73*, 103056. [CrossRef]
17. Sidiq, H.; Amin, R. Mathematical model for calculating the dispersion coefficient of super critical CO_2 from the results of laboratory experiments on enhanced gas recovery. *J. Nat. Gas Sci. Eng.* **2009**, *1*, 177–182. [CrossRef]
18. Sidiq, H.; Amin, R. The impact of pore pressure on CO_2-methane displacement. *Petrol. Sci. Technol.* **2012**, *30*, 2531–2542. [CrossRef]
19. Liu, S.-Y.; Ren, B.; Li, H.-Y.; Yang, Y.-Z.; Wang, Z.-Q.; Wang, B.; Xu, J.-C.; Agarwal, R. CO_2 storage with enhanced gas recovery (CSEGR): A review of experimental and numerical studies. *Pet. Sci.* **2022**, *19*, 594–607. [CrossRef]
20. Abba, M.K.; Al-Otaibi, A.; Abbas, A.J. Influence of permeability and injection orientation variations on dispersion coefficient during enhanced gas recovery by CO_2 injection. *Energies* **2019**, *12*, 2328. [CrossRef]
21. Zhang, Y.; Liu, S.; Chen, M.; Xu, S. Experimental study on dispersion characteristics and CH_4 recovery efficiency of CO_2, N_2 and their mixtures for enhancing gas recovery. *J. Nat. Gas Sci. Eng.* **2022**, *216*, 110756.
22. Honari, A.; Bijeljic, B.; Johns, M.L.; May, E.F. Enhanced gas recovery with CO_2 sequestration: The effect of medium heterogeneity on the dispersion of supercritical CO_2–CH_4. *Int. J. Greenh. Gas Con.* **2015**, *39*, 39–50. [CrossRef]

23. Nogueira, M.C.; Mamora, D.D. Effect of flue-gas impurities on the process of injection and storage of CO_2 in depleted gas reservoirs. *J. Energy Resour.-ASME* **2008**, *130*, 013301. [CrossRef]
24. Turta, A.T.; Sim, S.S.K.; Singhal, A.K.; Hawkins, B.F. Basic investigations on enhanced gas recovery by gas-gas displacement. *J. Can. Pet. Technol.* **2008**, *47*, 39–44. [CrossRef]
25. Sim, S.S.K.; Turtata, A.T.; Singhal, A.K.; Hawkins, B.F. Enhanced gas recovery: Factors affecting gas-gas displacement efficiency. *J. Can. Pet. Technol.* **2009**, *48*, 49–55. [CrossRef]
26. Liu, S.; Song, Y.; Zhao, C.; Zhang, Y.; Lv, P.; Jiang, L.; Liu, Y.; Zhao, Y. The horizontal dispersion properties of CO_2-CH_4 in sand packs with CO_2 displacing the simulated natural gas. *J. Nat. Gas Sci. Eng.* **2018**, *50*, 293–300. [CrossRef]
27. Mohammed, N.; Abbas, A.J.; Enyi, G.C.; Suleiman, S.M.; Edem, D.E.; Abba, M.K. Alternating N_2 gas injection as a potential technique for enhanced gas recovery and CO_2 storage in consolidated rocks: An experimental study. *J. Pet. Explor. Prod. Technol.* **2020**, *10*, 3883–3903. [CrossRef]
28. Wei, X.; Massarotto, P.; Wang, G.; Rudolph, V.; Golding, S.D. CO_2 sequestration in coals and enhanced coalbed methane recovery: New numerical approach. *Fuel* **2010**, *89*, 1110–1118. [CrossRef]
29. Pooladi-Darvish, M.; Hong, H.; Theys, S.; Stocker, R.; Bachu, S.; Dashtgard, S. CO_2 injection for enhanced gas recovery and geological storage of CO_2 in the Long Coulee Glauconite F Pool, Alberta. In Proceedings of the SPE Annual Technical Conference and Exhibition, Denver, CO, USA, 21–24 September 2008. SPE-115789-MS.
30. Zhang, H.; Pei, J.; Zhang, Y.; Jiang, C.; Zhu, J.; Ai, N.; Hu, Q.; Yu, J. Overpressure reservoirs of the Huangliu formation of the Dongfang area, Yinggehai basin, South China Sea. *Petrol. Explor. Dev.* **2013**, *40*, 305–315. [CrossRef]
31. Peters, E.J. *Advanced Petrophysics: Dispersion, Interfacial Phenomena*; Greenleaf Book Group: Austin, TX, USA, 2012.
32. Perkins, T.K.; Johnston, O.C. A review of diffusion and dispersion in porous media. *SPE J.* **1963**, *3*, 70–84. [CrossRef]
33. Delgado, J. Longitudinal and transverse dispersion in porous media. *Chem. Eng. Res. Des.* **2007**, *85*, 1245–1252. [CrossRef]